Phase synchronization in the perturbed Chua circuit

Murilo S. Baptista, Tiago P. Silva, José C. Sartorelli, and Iberê L. Caldas
Instituto de Física, Universidade de São Paulo, Caixa Postal 66318, 05315-970 São Paulo, São Paulo, Brazil

Epaminondas Rosa, Jr.
Department of Physics, Illinois State University, Normal, Illinois 61790-4560

(Received 27 November 2002; published 21 May 2003)

We show experimental and numerical results of phase synchronization between the chaotic Chua circuit and a small sinusoidal perturbation. Experimental real-time phase synchronized states can be detected with oscilloscope visualization of the attractor, using specific sampling rates. Arnold tongues demonstrate robust phase synchronized states for perturbation frequencies close to the characteristic frequency of the unperturbed Chua.

DOI: 10.1103/PhysRevE.67.056212 PACS number(s): 05.45.Vx, 05.45.Gg, 01.20.+x

I. INTRODUCTION

Synchronization refers to events that happen at the same time, as reported by Huygens in 1673 [1], describing periodic self-sustained synchronous states between two pendulum clocks. About three centuries later, a model proposed by Arnold [2] demonstrated that small periodic perturbations can produce stable periodic states in quasiperiodically oscillating systems. In the case of chaotic systems, it has been shown that a small, properly applied periodic perturbation, can force chaotic oscillations to get in phase with the perturbation, while the amplitude of the system's oscillation remains chaotic [3]. This phase synchronization effect can be viewed as a first step toward a more organized behavior of chaos, eventually leading the chaotic system to a periodic state. Phase synchronization has become a major field of interest with much work and applications [4].

Even though the extensive amount of study done on the perturbed Chua circuit [5], little is known about its phase synchronization process. In this paper, we demonstrate, both experimentally and numerically, that the properly paced Chua system is able to sustain states of robust phase synchronization with a periodic function. Moreover, the circuit oscillations remain phase synchronized for a range of bounded parameter perturbations, as required for the implementation of a communication scheme with chaos using the phase for encoding purposes [6].

We work with the chaotic oscillator in the single lobe regime (Rössler-like attractor), introduce the angle coordinate θ_{Chua} as a state space variable, and regard it as the phase of the Chua circuit. For the phase of the sinusoidal perturbation, we introduce θ_{pacer}. We say that the Chua and the pacer are phase synchronized when the phase difference $\Delta\theta = \theta_{Chua} - \theta_{pacer}$ remains bounded and small for all time (for details see Ref. [7]).

II. EXPERIMENTAL SETUP

The perturbed Chua circuit and the characteristic curve of the piecewise linear resistor R_{NL} are schematically shown in Fig. 1. This circuit is composed of two capacitors, C_1 and C_2, two resistors R and r, one inductor L, and the nonlinear (piecewise linear) resistor R_{NL}. The perturbation applied to the circuit is of the form $y(t) = V\sin(2\pi ft) = \mathrm{Im}(Ve^{i2\pi ft})$, where V is the amplitude and f is the perturbation frequency. We use a Tektronix AFG320 function generator that is connected in parallel to the resistor r of the circuit. An Agilent 35 670A dynamic signal analyzer is used to check the frequency f of the function generator, and also to measure the frequency f_0, based on a time series of V_{C1}. Data acquisition is performed using an AT-MIO 16E1 National Instruments board (12 bits) connected to a computer controlled by a software developed in LABVIEW. The dynamical variables of this circuit are the tension V_{C1} across the capacitor $C1$, the tension V_{C2} across the capacitor $C2$, and the current i_L across the inductor L. Due to the almost planar geometry of the Rössler-like attractor, we acquire only the variables V_{C1} and V_{C2}, which contains all the important information of this

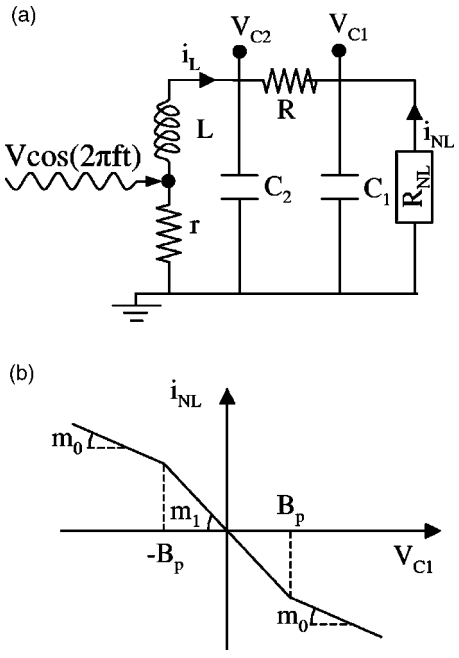

FIG. 1. (a) The Chua circuit, and (b) the piecewise linear characteristic curve of the resistor R_{NL}. The perturbation introduced is $V\sin(2\pi ft)$.

perturbed circuit. The R_{NL} characteristic curve is mathematically represented by $i_{NR}(V_{C1})=m_0V_{C1}+0.5(m_1-m_0)[|V_{C1}+B_p|+|V_{C1}-B_p|]$, where, $m_0=-0.539$, $m_1=-0.91$, and $B_p=1.2$V are the experimental values.

We work with Rössler-like attractors by setting suitable parameter values for the Chua circuit. The attractors can be represented well by the two-dimensional trajectory V_{C2} vs V_{C1} that spirals around an unstable saddle focus. The pacer can also be seen as a two-dimensional oscillator circling around the same focus.

III. REAL-TIME DETECTION OF PHASE SYNCHRONIZATION

Taking into account that both the chaotic circuit oscillation and the periodic function are basically two-dimensional rotations, the difference between their phases $\Delta\theta$ can be represented by the stroboscopic mapping of the perturbed circuit. This is done taking samples at $1/f$ time intervals, where f is the frequency of the periodic perturbation. The more compact the stroboscopic map, the less the variation of the phase difference. We say that the perturbed circuit is phase synchronized with its perturbation if the stroboscopic map remains constrict within a limited region of the attractor. Thus, for the sake of the present work, we consider the circuit to be phase synchronized with the perturbation if the stroboscopic map does not fill out all the region of the phase space in which the attractor lives in. In order to detect phase synchronization, we have to check whether the stroboscopic mapping on the variables V_{C1} and V_{C2}, sampled at frequency f, is confined into a subregion of the projection of the chaotic attractor on the plane V_{C1} vs V_{C2}. The characteristic frequency of the unperturbed circuit is $f_0=5.264$ kHz. We start the search for phase synchronized states by stroboscopically sampling the unperturbed Chua at frequency $f=f_0$. This is equivalent to starting with the pacer at frequency $f=f_0$ and amplitude V. The result is depicted in Figs. 2, where in (a) $f=f_0$ and $V=0.695$ mV. This amplitude value is not enough to produce phase synchronization so the points of the stroboscopic mapping, represented as open circles, are spread all over the attractor (pictured as a continuous circling gray line). As we increase the amplitude of the perturbation to, say $V=1.046$ mV, while maintaining the frequency at $f=f_0$, phase synchronization is attained, as indicated in Fig. 2(b). In this case, the stroboscopic mapping is confined to a subregion of the attractor, and remains there for all time. For higher amplitude of perturbation ($V=2.33$ mV), the stroboscopic mapping becomes more concentrated [see Fig. 2(c)] showing that the synchronization robustness increases with the amplitude of perturbation. Figure 3 illustrates the parameter space of $V\times f$, showing the triangular shaped area for which there is phase synchronization. We apply the technique described above for detecting whether or not phase synchronization occurs for a range of values of the amplitude V and the frequency f of the perturbation. We use 15 stroboscopic mappings with ≈ 6000 points each, for each value of V and f. The result is presented in Fig. 3, where the filled squares correspond to V and f values yielding phase synchronized states. The circle corresponds to the nonsynchronized state of Fig. 2(a), and the star and the triangle correspond to the phase synchronized states of Figs. 2(b) and 2(c), respectively. Notice the different slopes of the two sides of the tongue, with the curved right-hand side.

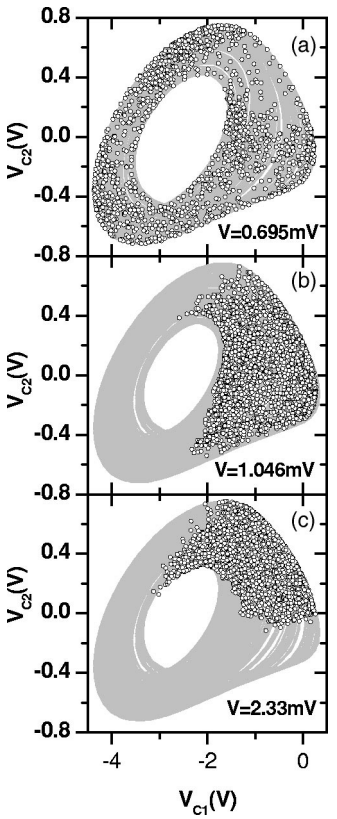

FIG. 2. Experimental data with $C_1=0.0047$ μF, $C_2=0.052$ μF, $R=1596$ Ω, $L=9.2$ mH, and $r=10$ Ω. Gray lines represent V_{C2} vs V_{C1} and empty circles represent the stroboscopic mapping. In (a) not synchronized with $V=0.695$ mV, in (b) phase synchronized with $V=1.046$ mV, and in (c) phased synchronized with $V=2.33$ mV. In all cases $f=f_0=5.264$ kHz.

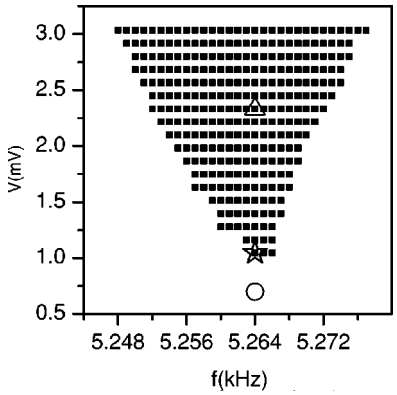

FIG. 3. Filled squares represent values of the frequency f and the amplitude V for which the experimental perturbed Chua circuit is phase synchronized with the perturbation. The open circle, the star and the triangle show the parameter space position used in Figs. 2(a–c), respectively.

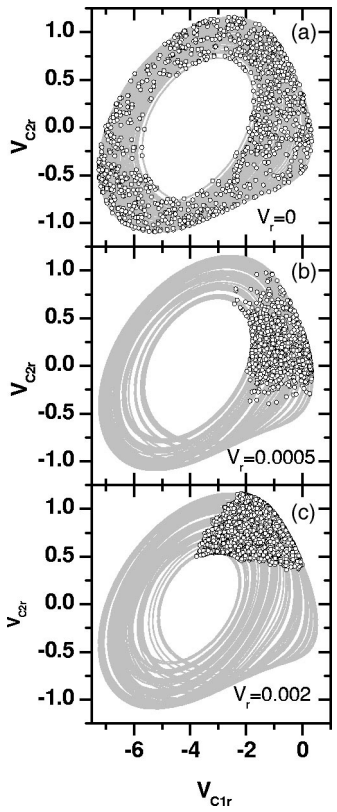

FIG. 4. The numerically simulated Chua circuit with dimensionless variables. The gray lines represent a Rössler-like attractor, while the empty circles represent the stroboscopic mappings. In (a) without perturbation there is no synchronization. In (b) perturbed with $f_r=0.2801$ and $V_r=0.0005$ there is sychronization. In (c) for higher amplitude perturbation $V_r=0.002$ the stroboscopic map is more concentrated.

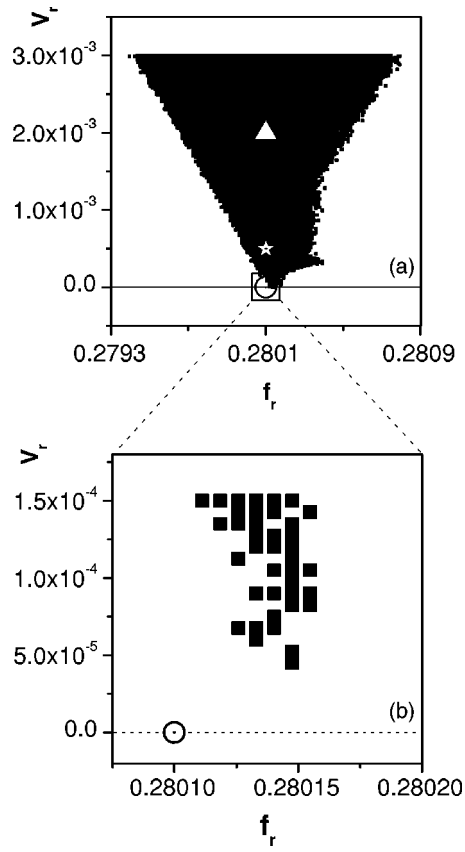

FIG. 5. In (a) the black region represents values of the frequency f_r and the amplitude V_r for which the numerically simulated perturbed Chua circuit phase synchronizes with the perturbation. The open circle, the star and the triangle show the values of V_r and f_r used to obtain the data shown in Figs. 4(a–c), respectively. In (b) a zooming view around $V_r=0$ and $f_r=0.2801$ showing the border of the synchronization tongue. The variables are dimensionless.

IV. SIMULATION

The experimental oscillator of Fig. 1 can be modeled by applying Kirchoff's laws to the nodes of the circuit. The resulting state equations are given by $C_1(dV_{C1}/dt)=(1/R)(V_{C2}-V_{C1})-i_{NR}(V_{C1})$, $C_2(dV_{C2}/dt)=(1/R)(V_{C1}-V_{C2})+i_L$, and $L(di_L/dt)=-V_{C2}-y(t)$, where V_{C1} and V_{C2} are the voltage across the capacitors C_1 and C_2, respectively, and i_L is the electric current across the inductor L. For convenience, we introduce the usual parameter rescaling that produces a set of dimensionless parameters (denoted with the subscript r). We permit a slight modification of the rescaled parameters due to fluctuations in the real experimental values. Thus, the parameters used in the numerical simulation of the circuit of Fig. 1 are $C_{1r}=0.1$, $C_{2r}=1.0$, $L_r=1/6$, $1/R_r=0.575$, $m_{0r}=-0.5$, $m_{1r}=-0.8$, and $B_{pr}=1.0$. The characteristic frequency of the Chua system for these parameters is $f_{0r}=0.2807$, which corresponds to the main peak in the Fourier spectrum [7].

Initial testing indicates that phase synchronization can be achieved for lower amplitude values when the frequency is $f_r=0.2801$, slightly different from the characteristic $f_{0r}=0.2807$. Our result for $V_r=0$ is shown in Fig. 4(a), where the stroboscopic mapping with sampling interval of 1/0.2801 is represented by the open circles plotted on top of the continuous Rössler-like attractor. As expected, the spread of the mapping around the attractor clearly indicates that the Chua oscillator and the sinusoidal function are not phase synchronized. However, a completely different picture can be seen when we increase the amplitude of the perturbation to $V_r=0.0005$, while keeping the frequency at $f_r=0.2801$. In this case, with the result displayed in Fig. 4(b), the open circles of the stroboscopic mapping are restricted to a bounded region of the attractor, and stay there for all time. The same sampling interval of 1/0.2801 has been applied for these mappings. We see that without the perturbation there is no phase synchronization due to the phase diffusion of the chaotic Chua. For $V_r=0.0005$, we already obtain phase synchronization as it is shown in Fig. 4(b). As shown for the experimental data, for higher amplitude of perturbation, $V_r=0.002$, the simulated stroboscopic map is also more concentrated [see Fig. 4(c)] confirming that the synchronization robustness increases with the amplitude of perturbation.

In Fig. 5(a), we show a 300×300 grid in parameter space of the perturbation frequency f_r and the perturbation amplitude V_r, showing in black square an Arnold-like tongue, a region for which phase synchronization occurs.

The open circle, the star and the triangle correspond, respectively, to the parameter settings of Figs. 2(a–c). As we observed in the experimental tongue, see Fig. 3, there is asymmetry between the left and the right borders of the tongue. In Fig. 5(b), we present a zooming view around $V_r = 0$ and $f_r = 0.2801$ showing a detail of the tip of the synchronization tongue.

V. PHASE SYNCHRONIZATION TRANSITION

The transition between phase synchronized and phase nonsynchronized states has been studied before. The scenario for the loss (or the achieving) of phase synchronization is equivalent to the loss (or achieving) of phase locking in a quasiperiodic oscillation, where a saddle-node bifurcation happens annihilating an attractor (node) and a repeller (saddle) [2]. In the case of states initially phase synchronized, synchronization is lost due to the collision of two sets. Depending on the particular system the synchronization loosing has also been described as a collision between an unstable set and an attractor [8], and as a collision between two unstable sets [9]. The tongue representing the parameter values for phase synchronization has been studied in association with chaotic systems [10]. It is a consequence of the finite probability of finding a rational periodic oscillation in a perturbed oscillator. In this sense, a very small perturbation amplitude, in connection with the characteristic frequency of the oscillator, is enough to lock the quasiperiodic (or chaotic) oscillations to the frequency of the forcing function. The finding of the Arnold tongue in both our experimental and simulation Chua circuits clearly indicates that this probability is indeed finite. Other types of electronic circuits producing chaotic wave signals may also be used for transmission of phase-coded information [11].

VI. CONCLUDING REMARKS

We have shown experimentally and numerically that the periodically perturbed Rössler-like chaotic Chua circuit phase synchronizes with the perturbation when the perturbing frequency is close to the characteristic frequency of the chaotic oscillator. Robust phase synchronized states are achieved for larger pacing amplitudes, which suggests that oscillators such as the Chua may offer some advantages for information transmission. The Arnold tongues for the experiment and the simulation are remarkably similar. In both cases, as we travel in the V vs f parameter space, three different regions can be visited. Take, for example, the Arnold tongue of Fig. 5. Suppose that we start at the left-hand side nonsynchronized position $f_r = 0.2793$, $V_r = 0.001$, and move to the right, increasing f_r at constant V_r. Eventually, we will reach the position $f_r = 0.279\,85$ close to the boundary between synchronization and nonsynchronization regions. As we continue with increasing values of f_r we cross the boundary, enter the region of phase synchronization, continue and reach the vicinity of the other boundary at $f_r = 0.280\,37$. As we continue, we cross this other boundary and travel again in nonsynchronization parameter space. Notice that the white regions to the left and to the right of the Arnold tongue correspond to parameter space values for nonsynchronized states. However, the left-hand side region corresponds to pacing frequencies lower than the characteristic frequency of the unperturbed Chua. The right-hand side region corresponds to pacing frequencies larger than the characteristic frequency of the unperturbed Chua. In one case the Chua is being forced to slow down, in the other case it is forced to speed up. For parameter values at the center of the tongue, going to the left slows the oscillator down, going to the right speeds it up. It seems that the chaotic oscillator reacts not exactly in the same way regarding the transition in one direction, as opposed to the transition in the other direction. These two diverse physical scenarios may account for the differences between the left-hand and right-hand sides of the Arnold tongue in both experimental and simulation cases.

ACKNOWLEDGMENTS

This work is partially supported by the Brazilian Agencies FAPESP and CNPq.

[1] C. Hugenii, *Horoloquim Oscilatorium* (Paris, France, 1673).

[2] V.I. Arnold, Trans. Am. Math. Soc. Ser. 2 **46**, 213 (1965).

[3] M.G. Rosenblum, A.S. Pikovsky, and J. Kurths, Phys. Rev. Lett. **76**, 1804 (1996).

[4] U. Parlitz, L. Junge, W. Lauterborn, and L. Kocarev, Phys. Rev. E **54**, 2115 (1996); D.Y. Tang, R. Dykstra, and N.R. Heckenberg, Phys. Rev. A **54**, 5317 (1996); P. Tass, M.G. Rosenblum, J. Weule, J. Kurths, A. Pikovsky, J. Volkmann, A. Schnitzler, and H.-J. Freund, Phys. Rev. Lett. **81**, 3291 (1998); P.M. Varangis, A. Gavrielides, T. Erneux, V. Kovanis, and L.F. Lester, *ibid.* **78**, 2353 (1997); J.R. Terry, K.S. Thornburg, Jr., D.J. DeShazer, G.D. Vanwiggeren, S. Zhu, P. Ashwin, and R. Roy, Phys. Rev. E **59**, 4036 (1999); A. Neiman, X. Pei, D. Russell, W. Wojtenek, L. Wilkens, F. Moss, H.A. Braun, M.T. Huber, and K. Voigt, Phys. Rev. Lett. **82**, 660 (1999); G.M. Hall, S. Bahar, and D.J. Gauthier, *ibid.* **82**, 2995 (1999); A.R. Yehia, D. Jeandupeux, F. Alonso, and M.R. Guevara, Chaos **9**, 916 (1999); J.-W. Shuai and D.M. Durand, Phys. Lett. A **264**, 289 (1999); V. Andrade, R.L. Davidchack, and Y.-C. Lai, Phys. Rev. E **61**, 3230 (2000); A. Dabrowski, Z. Gallias, and M. Ogorzalek, Int. J. Bifurcation Chaos Appl. Sci. Eng. **10**, 2391 (2000); D. Maza, A. Vallone, H. Mancini, and S. Boccaletti, Phys. Rev. Lett. **85**, 5567 (2000); D.J. DeShazer, R. Breban, E. Ott, and R. Roy, *ibid.* **87**, 044101 (2001); K. Josic and D.J. Mar, Phys. Rev. E **64**, 056234 (2001); Z. Zheng, X. Wang, and M.C. Cross, *ibid.* **65**, 056211 (2002); S. Rim, I. Kim, P. Kang, Y.-J. Park, and C.-M. Kim, *ibid.* **66**, 015205 (2002).

[5] M. Itoh, H. Murakami, and L.O. Chua, Int. J. Bifurcation Chaos Appl. Sci. Eng. **4**, 1721 (1994); L. Pivka, A.L. Zheleznyak, and L.O. Chua, *ibid.* **4**, 1743 (1994); M.S. Baptista and I.L. Caldas, Phys. Rev. E **58**, 4413 (1998); M.S. Baptista and I.L. Caldas, Nonlinear Dyn. **17**, 119 (1998); M.S.

Baptista and I.L. Caldas, Physica D **132**, 325 (1999).

[6] S. Hayes, C. Grebogi, E. Ott, and A. Mark, Phys. Rev. Lett. **73**, 1781 (1994); M.S. Baptista and L. Lopez, Phys. Rev. E **65**, 055201(R) (2002); M.S. Baptista, E. Rosa, Jr., M.B. Reyes, J.C. Sartorelli, Celso Grebogi, Int. J. Bifurcation Appl. Sci. Eng. Chaos (to be published).

[7] E. Rosa, Jr., W.B. Pardo, C.M. Ticos, J.A. Walkenstein, and M. Monti, Int. J. Bifurcation Chaos Appl. Sci. Eng. **10**, 2551 (2000); C.M. Ticos, E. Rosa, Jr., W.B. Pardo, J.A. Walkenstein, and M. Monti, Phys. Rev. Lett. **85**, 2929 (2000).

[8] A. Pikovsky, G. Osipov, M. Rosenblum, M. Zaks, and J. Kurths, Phys. Rev. Lett. **79**, 47 (1997).

[9] E. Rosa, E. Ott, and M.H. Hess, Phys. Rev. Lett. **80**, 1642 (1998).

[10] E.-H. Park, M.A. Zaks, and J. Kurths, Phys. Rev. E **60**, 6627 (1999); M.A. Zaks, E.-H. Park, M.G. Rosenblum, and J. Kurths, Phys. Rev. Lett. **82**, 4228 (1999).

[11] I.P. Marino, E. Allaria, R. Meucci, S. Boccaletti, and F.T. Arecchi, Chaos **13**, 286 (2003).